Semiclassical and quantum mechanical analysis of α-particle-induced reactions on praseodymium: A study relevant to precompound emission

Manoj Kumar Sharma,[1,*] M. M. Musthafa,[2] Mohd Shuaib,[3] Mahesh Kumar,[1] Vijay Raj Sharma,[4] Abhishek Yadav,[5] Pushendra P. Singh,[6] B. P. Singh,[3,†] and R. Prasad[3]

[1]*Department of Physics, Shri Varsheny College, Aligarh, Uttar Pradesh 202001, India*
[2]*Department of Physics, Calicut University, Calicut 673635, India*
[3]*Department of Physics, Aligarh Muslim University, Aligarh, Uttar Pradesh 202002, India*
[4]*Departamento de Aceleradores, Instituto Nacional de Investigaciones Nucleares, Apartado Postal 18-1027, CP 11801 Ciudad de Mexico, Mexico*
[5]*Inter University Accelerator Centre, New Delhi 110067, India*
[6]*Department of Physics, Indian Institute of Technology, Roopnagar Ropar, Punjab 140001, India*

(Received 20 August 2018; revised manuscript received 26 November 2018; published 9 January 2019)

Background: The study of precompound emission has attracted considerable attention for testing nuclear models in light-ion-induced reactions at relatively higher energies above 10 MeV/nucleon.
Purpose: Aiming to study the precompound emission and to develop systematics at low energies below 10 MeV/nucleon, where the compound emission process is likely to dominate, the excitation functions of the reaction residues produced in the interaction of α particles with ^{141}Pr have been measured in the energy range $\approx$14–40 MeV. Further, the measured data have been analyzed within the framework of both the semiclassical and quantum mechanical models.
Methods: The off-line γ-ray spectroscopy based stacked foil activation technique has been used to measure the excitation functions.
Results: The experimentally measured excitation functions have been compared with the theoretical predictions based on both the semiclassical model codes, viz., PACE4, TALYS-1.9, ACT, and ALICE91, and the quantum mechanical model code EXIFON. The analysis of the data shows that the experimental excitation functions could be reproduced only when the contribution of precompound emission, simulated theoretically, is taken into account. Further, the precompound fraction, which gives the relative importance of precompound emission over compound nucleus emission, has been deduced and is found to be energy dependent.
Conclusions: Analysis of data indicates that in α-induced reactions, the precompound emission plays an important role, even at the low incident energies, where the pure compound nucleus process is likely to dominate. The precompound fraction is found to strongly depend on the mass of the target nucleus and the excitation energy per surface nucleon of the composite system.

DOI: 10.1103/PhysRevC.99.014608

I. INTRODUCTION

The precompound (PCN) emission process that lies between compound nucleus (CN) and direct reaction (DR) mechanisms has been a topic of considerable importance in nuclear reaction dynamics at moderate excitation energies for many decades [1]. However, recent experimental evidences show the presence of PCN emission even at relatively low incident energies, where the CN process dominates. This has renewed interest in such studies for testing the nuclear models at low energies [1–3]. In the PCN process the emission of particles takes place during the redistribution of incoming particle energy among more and more nuclear degrees of freedom through a chain of particle-hole excitations prior to the establishment of statistical equilibrium [4–7]. Some of the important characteristics of the PCN process are (i) observation of a larger number of high-energy particles as compared to the spectrum predicted by the CN theory [8], (ii) forward-peaked angular distribution of the emitted particles [9], (iii) smaller value of velocity/recoil range/linear and angular momenta (spin) associated with the reaction residues left after emission of PCN particles as compared to CN particles [10], and (iv) slowly descending tail of the excitation functions (EFs) [1,4,5,11].

Furthermore, depending on the projectile energy, besides the PCN process, the CN and direct reaction processes are also dominant in light-ion-induced reactions. In the CN process the emission of light nuclear particles takes place after attaining statistical equilibrium, while the direct reactions occur at relatively higher energies where the reaction proceeds via the excitation of only a few degrees of freedom on a much shorter timescale, since the time taken by the projectile to

*Corresponding author: manojamu76@gmail.com
†bpsinghamu@gmail.com

travel across the target nucleus is much less than that in the case of the CN process. Generally total cross section for the production residues is taken as the sum of the CN, PCN, and DR contributions, neglecting all possible interference between them. However, the measured cross sections, in most cases, may be well explained on the basis of various nuclear models employing different optical potentials that make the study of the reaction dynamics to be of fundamental interest. The PCN plays a key role in the deexcitation of the composite excited system formed by the fusion of the projectile with the target leading to the evolution of equilibrium states of the compound nucleus.

In order to understand the PCN emission, the measured cross-section data for reactions induced by protons and α particles are rather more important than unstable nuclei, as they produce good-quality clean statistical data with the least background required for precise testing of the PCN models. The beams of light stable nuclei further decrease the probability of interferences of competing reaction mechanisms such as transfer, direct, and incomplete/breakup fusion reactions, as they have negligible probability for such reactions at the energy range of interest. The measurement and analysis of the EFs are of prime importance because the features of the EFs at low, medium, and high energies may give information about the reaction mechanism involved. The low-energy portion of the EFs is dominated by the CN mechanism; however, with the increase in projectile energy, the strength of the PCN process becomes relatively greater [12–16]. In addition to giving a better understanding of the reaction dynamics for developing the proper theories/models, the nuclear reaction data for neutron emission channels is also important for designing the nuclear energy generation devices such as the accelerator-driven subcritical (ADS) reactors [17].

Keeping in view the above, in the present work, EFs for the reactions ^{141}Pr$(\alpha, n)^{144}$Pm and ^{141}Pr$(\alpha, 2n)^{143}$Pm have been measured in the energy range ≈14–40 MeV. The analysis of experimentally measured EFs has been performed using theoretical model codes, viz., PACE4 [18,19], TALYS-1.9 [20], ACT [21,22], ALICE91 [23], and EXIFON [24]. The codes PACE4, TALYS-1.9, ACT, and ALICE91 are based on the semiclassical approach while the code EXIFON is based on multistep quantum mechanical theory.

The production cross section of ^{144}Pm and ^{143}Pm isotopes in the literature is scarce and is limited only to a few studies carried out for the measurements of cross sections relevant to utilization of accelerators by the proton and deuteron beams on ^{nat}Nd targets, respectively [25,26]. Lebeda *et al.* [25] measured the activation cross section for the residues ^{144}Pm in proton-induced reactions on the ^{148}Nd target in the energy range ≈10–30 MeV. Tarkanyi *et al.* [26] also measured the cross sections for the residues ^{144}Pm in deuteron-induced reactions on neodymium (^{nat}Nd) targets due to their therapeutic applications. Sauerwein *et al.* [27] studied the reaction ^{141}Pr$(\alpha, n)^{144}$Pm at the astrophysically relevant energies between 11.0 MeV and 15.0 MeV for testing optical-model potentials. It may, however, be pointed out that the EFs for the reaction residues ^{144}Pm and ^{143}Pm produced in ^{141}Pr(α, n) and ^{141}Pr$(\alpha, 2n)$ reactions were measured earlier [28] in almost the same energy region as that of the present work. They [28] analyzed the EFs for these reactions only with the code ALICE91 [23]. Further, their experimental cross section values were significantly different from the theoretical calculations, so much so that they [28] have to use a normalization constant to match the experimental and theoretical data. The use of this normalization constant has no physical reasoning and, therefore, the authors [28] themselves recommended further investigation of this case. In view of the above, the remeasurement of excitation functions for the reactions ^{141}Pr$(\alpha, n)^{144}$Pm and ^{141}Pr$(\alpha, 2n)^{143}$Pm are required for testing various theoretical semiclassical and quantum mechanical models.

This paper is organized as follows: The experimental details of the measurements of EFs are given in Sec. II, while Sec. III deals with the model calculations. A discussion on the systematic study of precompound emission by deducing precompound fraction f_{pe} is given in Sec. IV, while the conclusions drawn from the present analysis are summarized in Sec. V.

II. MEASUREMENTS OF EXCITATION FUNCTION

A well-collimated α-particle beam obtained from the Variable Energy Cyclotron Centre (VECC), Kolkata, India, has been used to perform the experiments for the measurement of excitation functions for the production of radioisotopes in the interaction of natural praseodymium (^{141}Pr) as targets. The spectroscopically pure, ^{141}Pr target material of thickness ≈3.32 mg/cm^2 was deposited on the Al foils of thickness ≈6.75 mg/cm^2 by using the vacuum evaporation technique. The Al foils served both as energy degrader and catcher/backing foils, where the recoiling residues from the composite system may be trapped. The thickness of each target sample/Al-catcher was determined precisely prior to its use in the stack by the α-transmission method, which is based on the measurement of the energy lost by 5.487 MeV α particles, obtained from a standard ^{241}Am source, while passing through the target material. In the stacked foil activation technique, the energetic beam of α particles traverses through the samples with degrading beam energies. Thus, it is possible to bombard the samples of a stack at different energies in a single irradiation.

In the present experiment, a stack consisting of eight ^{141}Pr target-catcher assembles was irradiated for ≈12 h. The beam current ≈100 nA was monitored from the current integrator count rate. The calculations of average beam energy on a given target of the stack have been performed using the stopping power program SRIM [29]. The postirradiation analysis has been carried out by using a high-resolution large-volume (100 cc) high-purity germanium (HPGe) detector coupled to an ORTEC's PC based multichannel analyzer. In the present work, a ^{152}Eu point γ source is used to determine the efficiency of the HPGe detector. The geometry-dependent efficiency (G_ε) of the HPGe detector for different source-detector separations was estimated using following relation:

$$G_\varepsilon = \frac{D_0}{D_M I_\gamma e^{-\lambda t}}, \tag{1}$$

where D_0 is the observed disintegration rate of the standard source at the time of measurement, D_M is the disintegration

TABLE I. List of reactions and their spectroscopic data.

Reactions	Q Value (MeV)	Half-Life (days)	E_γ (keV)	Branching Ratio (%)
^{141}Pr$(\alpha, n)^{144}$Pm	−10.25	363	476.81	42.2
			618.06	99.1
			696.54	100.0
^{141}Pr$(\alpha, 2n)^{143}$Pm	−16.77	265	741.98	38.5

rate at the time of manufacture, λ is the decay constant, t is the lapse time between the manufacture of the source and the start of counting, and I_γ is the branching ratio of the characteristic γ rays.

The resolution of the HPGe detector system was ≈2 keV for the 1332 keV γ line of ^{60}Co. During the counting of the samples, the sample-detector distances are suitably adjusted in order to minimize the dead time to <10%. The pertinent decay data such as the energy of the characteristic γ rays, half-lives, and branching ratios of residual nuclei produced in the $\alpha + {}^{141}$Pr system for the yield calculations were taken from Ref. [30] and are given in Table I. It may be pointed out here that the residues are identified by their characteristic γ rays and measured half-lives. The measured intensities of the characteristic γ lines of the identified residues have been used to calculate the cross sections for the corresponding reaction channels employing a FORTRAN program based on standard formulations [16],

$$\sigma_r(E) = \frac{C_a \lambda \exp(\lambda t_l)}{N_0 \phi P K(G_\varepsilon)[1-\exp(-\lambda t_i)][1-\exp(-\lambda t_a)]}, \tag{2}$$

where C_a is the observed counts during the accumulation time t_a of the induced activity of decay constant λ, N_0 the number of target nuclei irradiated for time t_i with a particle beam of flux ϕ, t_l the time lapse between the stop of irradiation and the start of counting, P the branching ratio of the characteristic γ ray, and G_ε is the geometry-dependent efficiency of the detector for the γ ray of a given energy. The value of G_ε depends on the energy of the γ ray and also on the relative separation between the source and detector. A typical γ-ray spectrum of a standard source ^{152}Eu of known strength, recorded prior to actual experiment for α-induced reactions ^{144}Pm at source-detector distance 3 cm, is shown in Fig. 1. In order to determine the value of G_ε for γ rays of different energies, a standard source of ^{152}Eu of known strength was used. As such, proper correction for the geometry-dependent efficiency has been taken into account for each case. The factor $[1-\exp(-\lambda t_i)]$, known as the saturation correction, takes care of the decay of evaporation residues during the irradiation. The corrections for the decay of the induced activity due to the delay between the stop of irradiation and the start of counting and during the data accumulation are taken into account via the factors $\exp(\lambda t_l)$ and $[1-\exp(-\lambda t_a)]$, respectively. $K = [1-\exp(-\mu x)]/\mu x$ is the correction for the self-absorption of the γ radiation in the sample thickness itself, where x is the thickness of the sample and μ is the γ-ray absorption coefficient. It may be pointed out that the

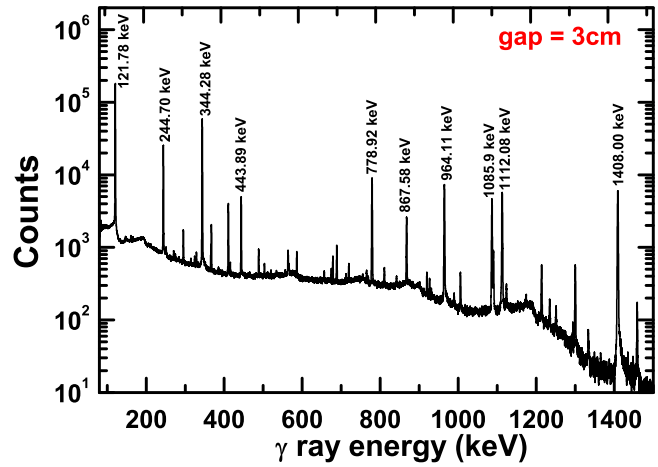

FIG. 1. A typical γ-ray spectrum of a standard source ^{152}Eu of known strength, recorded prior to actual experiment for α-induced reactions ^{144}Pm at source-detector distance (gap) 3 cm.

dead time of a spectrometer is a very sensitive parameter that can effect the measured cross section substantially. Therefore, it is required to apply proper correction to the experimental data for dead time. As a representative case, Fig. 2 shows the variation of geometry-dependent efficiency [calculated using Eq. (1)] with γ-ray energy in the range 121.7 keV to 1408 keV for a standard ^{152}Eu gamma source of known strength at a source-detector distance of 3.0 cm with proper dead-time corrections.

A critical evaluation of uncertainties in the measured cross sections (as given in Table II) has been considered and is estimated to be <10%. The errors in the measured cross sections may arise due to (a) nonuniform deposition of the target material and inaccurate estimate of the foil thickness which may be ⩽1%, and (b) the fact that during the irradiations, fluctuations in the beam current may result in the variation of the incident flux. Many tests were performed to check the time-integrated beam fluctuations and it was

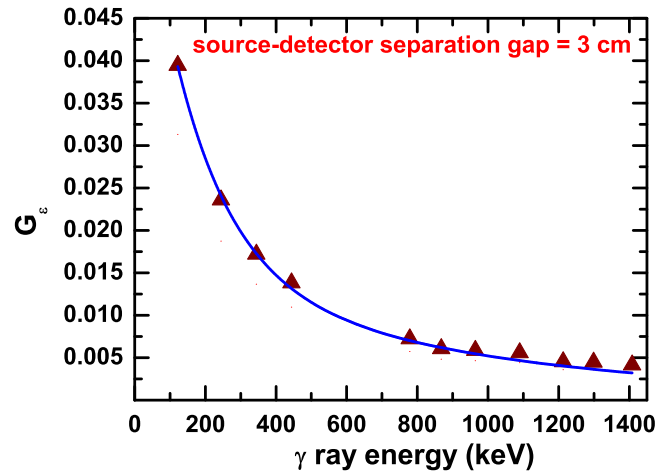

FIG. 2. The curves for geometry-dependent efficiency with proper dead-time correction obtained from a standard source ^{152}Eu of known strength at source-detector distance 3 cm.

TABLE II. Experimentally measured cross sections.

E_α (MeV)	$\sigma(^{144}\mathrm{Pm})$ (mb)	$\sigma(^{143}\mathrm{Pm})$ (mb)
14.2 ± 1.2	24.6 ± 4.4	
15.7±0.9 Ref. [28]	19.9 ± 3.2	
16.5±1.0	123.8 ± 18.9	
18.2±0.9 Ref. [28]	139.8 ± 17.8	168.1 ± 21.2
18.6±0.9	156.8 ± 21.2	122.8 ± 21.5
21.9±0.9	55.1 ± 9.0	350.7 ± 55.3
25.9±0.8 Ref. [28]	21.3 ± 3.8	472.5 ± 56.7
27.2±0.8	25.2 ± 4.2	572.8 ± 84.4
30.1±0.79 Ref. [28]	11.9 ± 2.4	191.8 ± 23.6
31.9±0.7	14.6 ± 3.3	541.5 ± 82.9
35.9±0.74 Ref. [28]	10.0 ± 2.10	99.5 ± 12.6
36.1±0.6	10.1 ± 2.2	252.3 ± 41.4
40.0±0.6	7.8 ± 1.9	113.8 ± 19.1
44.5±0.7 Ref. [28]	5.2 ± 1.70	66.6 ± 9.7

estimated that beam fluctuations may introduce errors of not more than 5% in the measured cross sections. Other sources of error include that (c) uncertainty in the determination of the geometry-dependent efficiency of the γ-ray spectrometer may give rise to error in the production cross sections. Further, the uncertainty in determining the efficiency of the spectrometer may also appear due to the solid-angle effect, as the irradiated samples were not point sources like the standard source, but had a finite diameter, which may be $\leqslant$5%. (d) The product nuclei recoiling out of the thin target may introduce large errors in the measured cross sections. This was minimized as the catcher/backing foils used in the stack for irradiation were of sufficient thickness to stop even the most energetic recoiling residues.

III. MODEL CALCULATIONS

In the present work, the theoretical calculations for cross sections have been performed employing both the semiclassical codes, viz., PACE4 [18,19], TALYS-1.9 [20], ACT [21], and ALICE91 [23], as well as the code EXIFON [24], which is based on multistep quantum mechanical (QM) theory [31–34]. Brief details of these codes are given in the following subsections.

A. Calculations with the code PACE4

Theoretical calculations with the code PACE4 [18,19] have been performed by using Bass formulations [35], which are based on the Hauser-Feshbach (HF) formalism and follow the Monte Carlo simulation. For compound nucleus formation, at a particular angular momentum ℓ and specific bombarding energy E, the partial cross section σ_ℓ is given by

$$\sigma_\ell = \frac{\lambda^2}{4\pi}(2\ell+1)T_\ell, \tag{3}$$

where λ is the reduced wavelength and the transmission coefficients T_ℓ may be given by the expression

$$T_\ell = \left[1+\exp\left(\frac{\ell-\ell_{\max}}{\Delta}\right)\right]^{-1}, \tag{4}$$

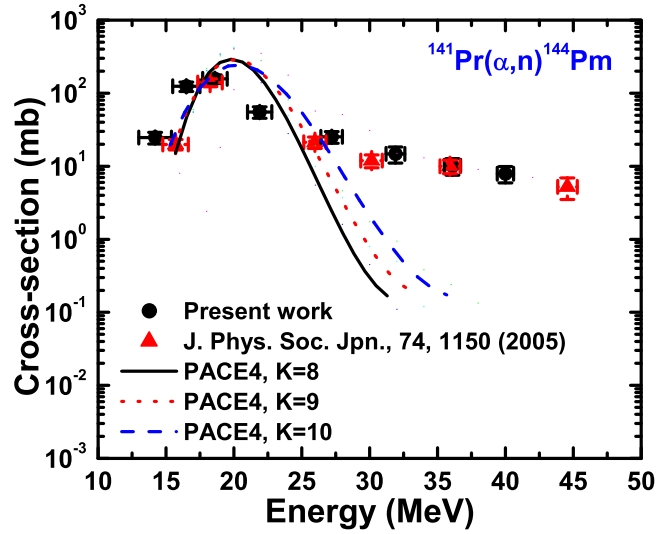

FIG. 3. The experimentally measured and theoretically calculated EFs for reaction $^{141}\mathrm{Pr}(\alpha, n)^{144}\mathrm{Pm}$ using code PACE4. The effect of variation of parameter K (=8, 9, and 10) on PACE4 calculations is also shown in this figure. See text for details.

where Δ is the diffuseness parameter, while $\ell_{\max}$ is the maximum value of ℓ determined by the total fusion cross section,

$$\sigma_F = \sum_{\ell=0}^{\infty}\sigma_\ell. \tag{5}$$

In this code, level density parameter a $(= A/K)$ is an important parameter which governs the shape of excitation function through the evaporation process. Here, A is the mass number of the compound nucleus and K is a free parameter which may be varied to match the experimental data.

The experimentally measured and theoretically calculated EFs for reactions $^{141}\mathrm{Pr}(\alpha, n)^{144}\mathrm{Pm}$ and $^{141}\mathrm{Pr}(\alpha, 2n)^{143}\mathrm{Pm}$ are shown in Figs. 3 and 4, respectively. The effect of variation of parameter K (=8, 9, and 10) on PACE4 calculations has also been shown in these figures. As can be seen from these figures, a value of $K = 8$ (default value) is found to satisfactorily reproduce the experimentally measured reaction cross sections particularly up to the peak region. The experimentally measured values by Ansari *et al.* [28] for these reactions are also indicated in Figs. 3 and 4, respectively. The enhancement of the experimental cross sections as compared to PACE4 calculations has been observed towards higher projectile energies, i.e., in the tail portion of EFs. It may be pointed out that this observed enhancement in the experimental EFs for reaction $^{141}\mathrm{Pr}(\alpha, n)^{144}\mathrm{Pm}$ above projectile energy 25 MeV could not be reproduced by changing the values of K in PACE4 calculations. This is expected since code PACE4 takes into account evaporation reaction channels proceeding only via CN process; therefore, the observed experimental enhancement in EFs as compared to PACE4 calculations clearly indicates that this reaction channel may have significant contributions from the processes other than the CN process. It may be remarked that the contribution of the direct reaction to the same reaction residues is expected to be negligible at these energies. Hence,

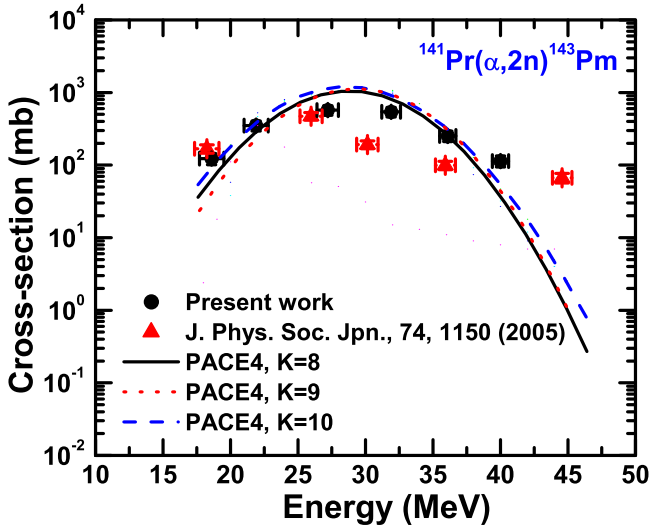

FIG. 4. The experimentally measured and theoretically calculated EFs for reaction ^{141}Pr(α, 2n)^{143}Pm using code PACE4. The effect of variation of parameter K (=8, 9, and 10) on PACE4 calculations is also shown in this figure.

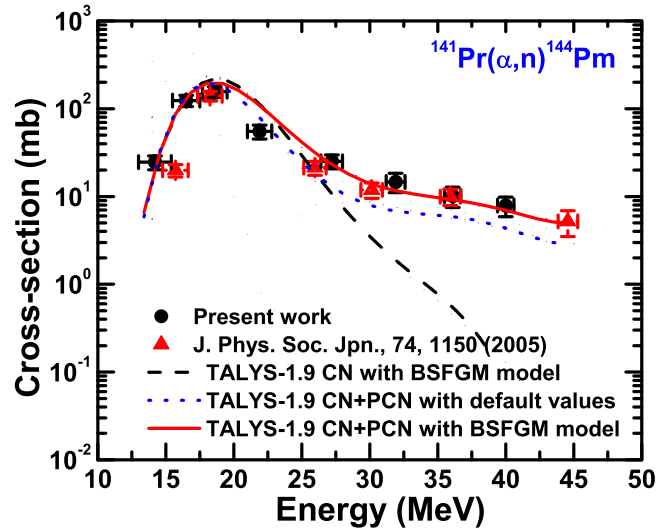

FIG. 5. The experimentally measured and theoretically calculated EFs for reaction ^{141}Pr(α, n)^{144}Pm using code TALYS-1.9. See text for details.

observed enhancement of the experimental cross sections in the tail portion of EFs for reaction ^{141}Pr(α, n)^{144}Pm as compared to the theoretical calculations may be attributed to the PCN emission process, which is a dominant mode of mechanism in one neutron emitting reaction channel. For reaction ^{141}Pr(α, 2n)^{143}Pm, the experimentally measured EFs are well reproduced by PACE4 calculations up to ≈35 MeV, while above this energy, the enhancement of experimental cross sections as compared to PACE4 calculations may be explained due to the contribution of the PCN process.

B. Calculations with the code TALYS-1.9

The theoretical model code TALYS-1.9 [20] is one of the most updated codes which is used to calculate the cross section for residues produced in light-particle (proton and alpha) induced reactions up to projectile energies 200 MeV [36–38]. The reaction parameters in this model code are taken from the RIPL database [39]. One of the most important advantages of this code is that it predicts the cross section for the residues produced considering the compound, the precompound, and direct reaction mechanisms. In this model, the optical parameters obtained from a global potential of Koning and Delaroche [40] are taken into account. The compound nucleus reaction mechanism has been incorporated by using the Hauser-Feshbach (HF) theory [41]. The exciton model developed by Kalbach [42] has been used to determine the precompound contribution. The different level densities used account for the constant-temperature Fermi gas model (CTFGM) [43], back-shifted Fermi gas model (BSFGM) [44], generalized superfluid model (GSFM) [45,46], microscopic level densities from Goriely's and Hilaire's tables [47], and microscopic level densities (temperature-dependent Hartree-Fock-Bogoliubov (HFB), Gogny force) [48]. In the present work, the theoretical calculations have been performed for reactions ^{141}Pr(α, n)^{144}Pm and ^{141}Pr(α, 2n)^{143}Pm by using different options of the code TALYS-1.9. A comparison of calculations performed for CN (shown by dashed line) and CN+PCN (shown by dotted and solid lines) processes of this code along with experimentally measured cross sections for the reactions ^{141}Pr(α, n)^{144}Pm and ^{141}Pr(α, 2n)^{143}Pm are shown in Fig. 5 and Fig. 6, respectively. It can been seen from Fig. 5 that the CN calculations based on Hauser—Feshbach theory reproduce the experimental data for reaction ^{141}Pr(α, n)^{144}Pm up to the peak region, indicating contributions from other reaction mechanisms at higher energies. When the precompound contribution has been taken into account by using the constant-temperature Fermi gas model (default option) of the code TALYS-1.9, it has been found that the trend of the

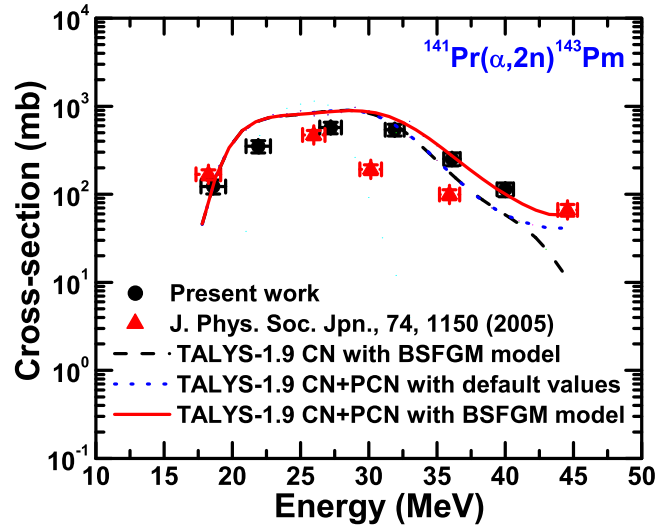

FIG. 6. The experimentally measured and theoretically calculated EFs for reaction ^{141}Pr(α, 2n)^{143}Pm using code TALYS-1.9. See text for details.

theoretical calculations follows the experimental data. However, at higher energies the experimentally measured values of the cross section are relatively larger as compared to the precompound calculations with the default option of this code. An attempt has also been made to reproduce the experimental data in the tail portion (towards the higher projectile energies) of the measured EFs by using a different level density from the other option of the code TALYS-1.9, as discussed above. It has been found that the calculations performed for the reactions ^{141}Pr$(\alpha, n)^{144}$Pm and ^{141}Pr$(\alpha, 2n)^{143}$Pm with the back-shifted Fermi gas model (BSFGM) [44] of the code TALYS-1.9, as shown in Fig. 5 and Fig. 6 by a solid line, are in good agreement with the experimental data. This is expected, since in the BSFGM [44] model, the pairing energy is treated as an additional parameter with the Fermi gas model that increases the value of the level density and hence may have a larger contribution due to the precompound emission.

C. Calculations with the code ACT

The theoretical calculations for the excitation functions have been performed using the code ACT [21] which is based on the lines of code STAPRE [22]. In this code, each evaporation step is treated within the framework of a statistical model with consideration of angular momentum and parity conservation. For the emission of the first particle, PCN decay is also taken into the account. In this code the CN calculations are performed using the HF model [41], while the exciton model is employed for the simulation of PCN emission. The level densities are calculated within the framework of the back-shifted Fermi gas model by the spin-dependent Lang expression [49]. The effective moment of inertia Θ_{eff} is taken consistently equal to the rigid-body value in these calculations. The transmission coefficients required in the calculations are generated by using the global optical model potentials [50]. The separation energies needed in these calculations are taken from the tables of Wapstra and Bos [51], and the decay scheme of various nuclei from the *Table of Radioactive Isotopes* [30]. The transition rates λ_+, λ_0, and λ_- are related by the Williams expression [52] and corrected for the Pauli principle by Cline [53]:

$$\lambda_+ = \frac{2\pi}{\hbar}|\bar{M}|^2 \frac{g^3}{U^2}(n+1), \tag{6}$$

$$\lambda_0 = \frac{2\pi}{\hbar}|\bar{M}|^2 g n_p n_h (n-2), \tag{7}$$

$$\lambda_- = \frac{2\pi}{\hbar}|\bar{M}|^2 g^2 U \frac{(3n-2)}{4}. \tag{8}$$

In this model the states of the system are classified according to the number of excitons i.e., the number of excited particle n_{p} and hole n_{h} degrees of freedom, respectively. The application of a two-body interaction to the state of a $(n_{\text{p}}, n_{\text{h}})$ configuration leads to states with $(n_{\text{p}}+1, n_{\text{h}}+1)$, $(n_{\text{p}}, n_{\text{h}})$, or $(n_{\text{p}}-1, n_{\text{h}}-1)$ excited particles and holes.

In order to evaluate internal transition rates it is necessary to calculate the absolute value of the square of the average matrix element $(|\bar{M}|^2)$ [54] by the expression $|\bar{M}|^2 = F_M A^{-3} U^{-1}$ [55], where A is the mass number and U the excitation energy of the composite system. Here, F_M is a constant and is treated as an adjustable parameter to match the experimental data. In the present work, the value of F_M is taken as 430 MeV^3, as used consistently in our earlier work [4], and is found to satisfactorily reproduce the experimental data in the present case also.

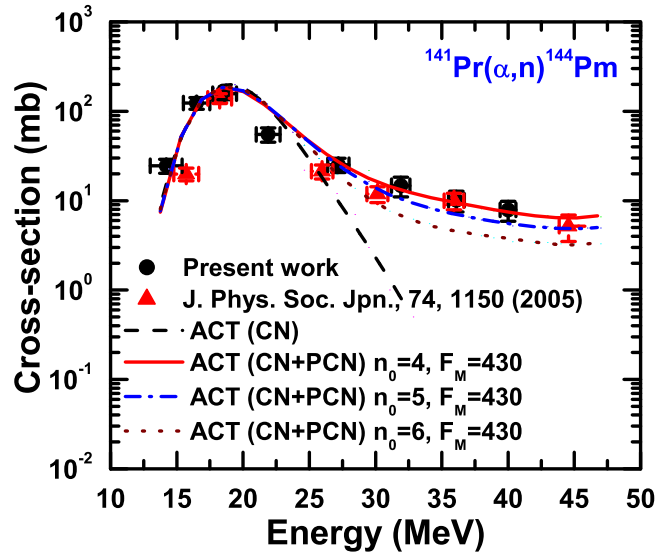

FIG. 7. The experimentally measured and theoretically calculated EFs for reaction ^{141}Pr$(\alpha, n)^{144}$Pm using code ACT. The effect of variation of parameter n_0 (=4, 5, and 6) is shown in this figure. The best choice of parameters n_0 is discussed in text.

Another important parameter of the code ACT that governs the PCN component is initial exciton number n_0 $(=n_{\text{p}} + n_{\text{h}})$. The calculations have been performed using different values of the initial exciton number $n_0 = 4$ $(2p + 2n + 0\text{h})$, $n_0 = 5$ $(3p + 2n + 0\text{h})$, and $n_0 = 6$ $(3p + 2n + 1\text{h})$, respectively. Keeping the value of $F_M = 430$ MeV^3, the effect of variation of the n_0 on measured EFs for reactions ^{141}Pr$(\alpha, n)^{144}$Pm and ^{141}Pr$(\alpha, 2n)^{144}$Pm is shown in Figs. 7 and 8, respectively along with their CN calculations. It can be seen from Figs. 7 and 8 that a value of initial exciton number $n_0 = 4$ fits the experimental data satisfactorily over the entire energy range for both the reactions ^{141}Pr$(\alpha, n)^{144}$Pm and ^{141}Pr$(\alpha, 2n)^{143}$Pm. A value of initial exciton number $n_0 = 4$ for α-induced reactions is justified [56]. The lower value of initial exciton number n_0 gives larger PCN contributions. It is because of the fact that the lower value of n_0 means larger number of two-body interactions prior to the establishment of thermodynamic equilibrium, resulting in a larger PCN contribution.

In light of the above discussion, when the calculations of cross sections are performed by the code ACT using the compound nucleus model, it has been observed that the high-energy tail portion of measured excitation functions is overestimated as compared to their theoretical values. However, when the PCN contribution is added to the CN calculations, it has been found, in general, that there is a satisfactory reproduction of the experimental data for the presently measured excitation functions. As such, the above analysis indicates

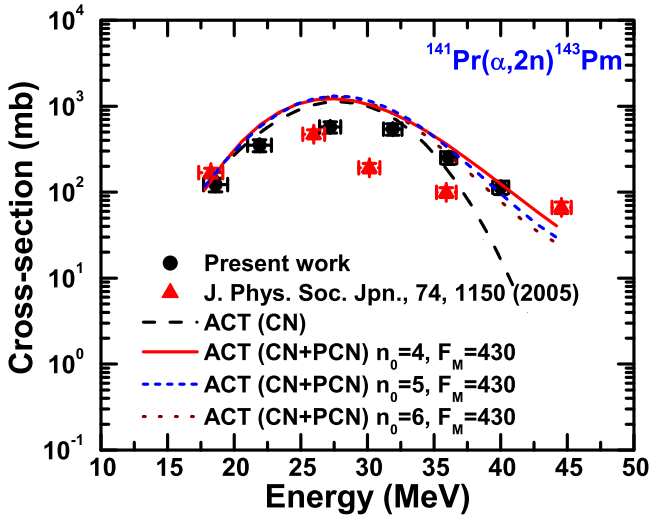

FIG. 8. The experimentally measured and theoretically calculated EFs for reaction ^{141}Pr$(\alpha, 2n)^{143}$Pm using code ACT. The effect of variation of parameter n_0 (=4, 5, and 6) is shown in this figure.

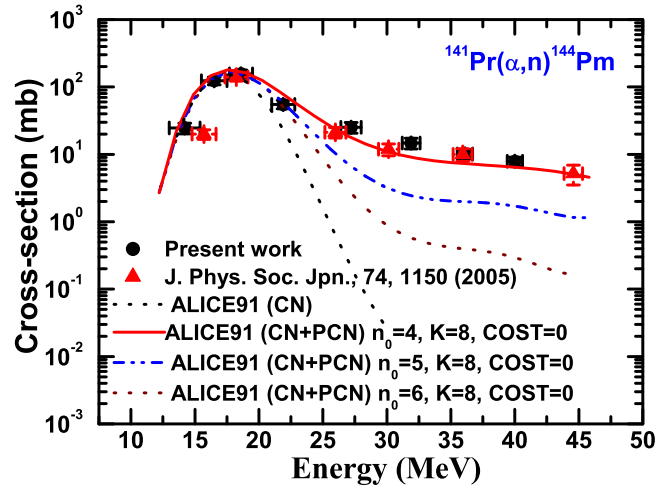

FIG. 9. The experimentally measured and theoretically calculated EFs for reaction ^{141}Pr$(\alpha, n)^{144}$Pm using code ALICE91. The effect of variation of parameter n_0 (=4, 5, and 6) is shown in this figure. The details of the parameter n_0 are discussed in the text.

that there is a significant contribution expected from PCN emission for these channels at higher energies.

D. Analysis of excitation functions with code ALICE91

The code ALICE91 developed by Blann [23] has been used to calculate the cross sections for CN and PCN emissions based on the Weisskopf-Ewing model [57] and the geometry-dependent hybrid model [56], respectively. The Myers-Swiatecki/Lysekil mass formula [58] is used for calculating the Q values and the binding energies of all the nuclei in the evaporation chain. The inverse reaction cross sections used in the code are calculated using an optical model [59] subroutine. The calculations for the PCN emission in this code are performed assuming equipartition of energy among initially excited particles and holes. The mean-free path for intranuclear transition rates may be calculated either from the optical potential parameters of Becchetti and Greenlees [60] or from Pauli-corrected nucleon-nucleon cross sections [61,62].

In this code, the level density parameter a, the initial exciton number n_0, and the mean-free path multiplier COST are some of the important parameters. The level density parameter a mainly affects the CN component, while the initial exciton number n_0 and the mean-free path multiplier COST govern the PCN component. The level density parameter may be calculated as $a = A/K$, where A is the mass number of the composite nucleus and K is an adjustable parameter [63] which can be varied to match the measured EFs. The CN calculations of the code ALICE91 are performed by taking the value of $K = 8$ (default value), which gives satisfactorily the reproduction of the experimentally measured EFs in the peak region as shown in Fig. 9 for reaction ^{141}Pr$(\alpha, n)^{144}$Pm. As mentioned, the level density parameter a mainly governs the CN component; hence, the tail portion of EFs could not be reproduced by varying the value of the parameter K.

Further, in the geometry-dependent hybrid model, the initial configuration of the compound system defined by the exciton number n_0 ($=n_p + n_h$) is a crucial parameter of the PCN formalism. In order to get an actual value of the initial exciton number n_0, the calculations for different values of n_0 ranging from 4 to 6 with configurations $n_0 = 4$ ($2p + 2n + 0h$), $n_0 = 5$ ($3p + 2n + 0h$), and $n_0 = 6$ ($3p + 2n + 1h$), respectively, have been performed for reactions ^{141}Pr$(\alpha, n)^{144}$Pm and ^{141}Pr$(\alpha, 2n)^{143}$Pm and are shown in Figs. 9 and 11, respectively. It may be observed from these figures that a value of initial exciton number $n_0 = 4$ fits the experimental data satisfactorily over the entire range of energies.

The mean-free path multiplier COST is another parameter of the ALICE91 which is used to adjust the nuclear mean-free path to reproduce the experimental data. This accounts for the difference, if any, between the calculated and actual mean-free paths for two-body residual interactions. The effect of variation of parameter COST, i.e., COST=0 (default value) and COST=2, on the calculated EF for the reaction ^{141}Pr$(\alpha, n)^{144}$Pm is shown in Fig. 10. As can be seen from this figure, a value of COST=2 along with $K = 8$ and $n_0 = 4$ gives the best fit to the experimental data over the entire range of projectile energies. The ALICE91 calculations have also been performed for reaction ^{141}Pr$(\alpha, 2n)^{143}$Pm using the same set of parameters and are shown in Fig. 11. As can be seen from this figure the shape of the EFs for this reaction is satisfactorily reproduced using the code ALICE91, as well.

E. Analysis of excitation functions with code EXIFON

The code EXIFON [24] is based on an analytical model for statistical multistep direct and multistep compound reactions (SMD/SMC model) [64]. It predicts the activation cross section including the equilibrium and precompound as well as the direct (collective and noncollective) processes within a pure statistical multistep reaction model. The initial exciton number n_0 in this code is taken equal to 4 for α-induced

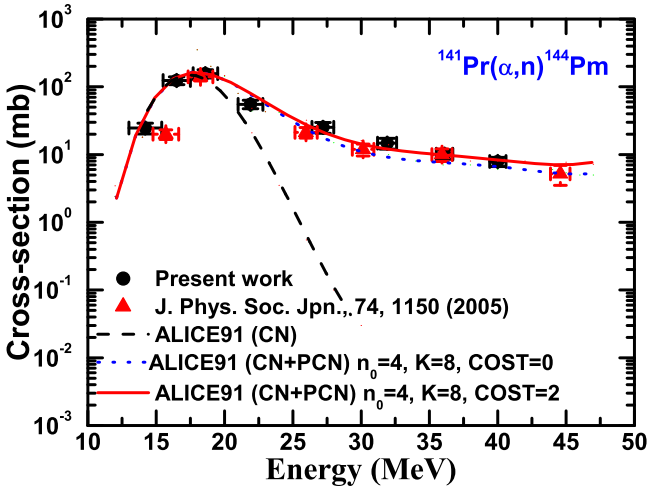

FIG. 10. The experimentally measured and theoretically calculated EFs for reaction ^{141}Pr$(\alpha, n)^{144}$Pm using code ALICE91. The effect of variation of parameter COST is shown in this figure. See text for details.

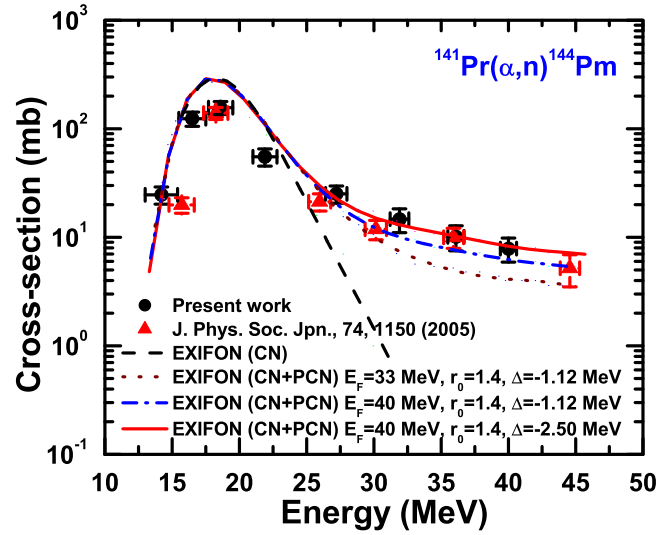

FIG. 12. The experimentally measured and theoretically calculated EFs for reaction ^{141}Pr$(\alpha, n)^{144}$Pm using code EXIFON. The effect of variation of parameter Δ on theoretical calculations is also shown.

reactions, similarly to the one taken in semiclassical calculations performed by ACT and ALICE91. The calculation with the code EXIFON takes into account the pairing correction, Pauli blocking, shell structure, and the Coulomb effects.

The experimentally measured and theoretically calculated EFs for reactions ^{141}Pr$(\alpha, n)^{144}$Pm and ^{141}Pr$(\alpha, 2n)^{143}$Pm using the code EXIFON with different sets of parameters are shown in Fig. 12 and Fig. 13, respectively. It can be observed from these figures that the calculations performed using the standard set of parameters underestimates the experimental data, particularly in the tail portion. In order to match the experimental data the values of some of the parameters have been varied from that of the standard set. The value of the pairing correction term has been changed from −1.12 (standard value) to −2.5 which is in agreement with the value used by Kalbach-Cline, Huizenga, and Vonach [65] and Coryell [66]. The Fermi energy E_F is related to the single-particle state density g and through it to the level density parameter a. For $E_F = 40$ MeV, using the formulation of Kalbach [67–70], Oblozinky [71], and Avrigeanu *et al.* [72,73] one gets the value of $a = 8$ along with with radius parameter $r_0 = 2.25$ fm. These values of E_F (=40 MeV) and r_0 (=2.25 fm) are used in the present calculations and give satisfactory reproduction of experimentally measured EFs for reactions ^{141}Pr$(\alpha, n)^{144}$Pm

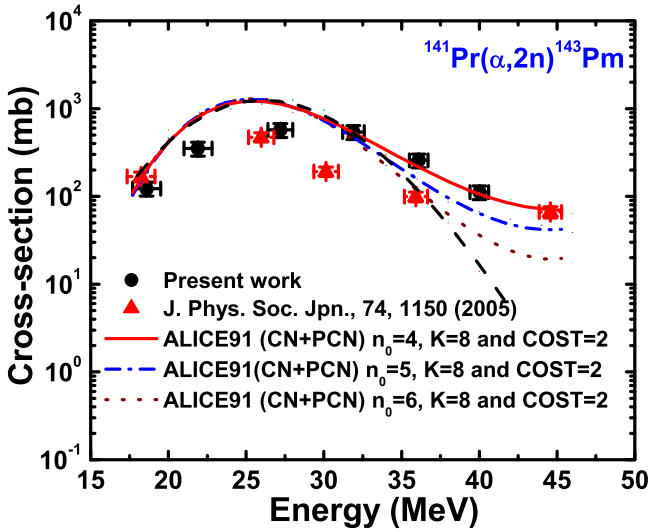

FIG. 11. The experimentally measured and theoretically calculated EFs for reaction ^{141}Pr$(\alpha, 2n)^{143}$Pm using code ALICE91. The effect of variation of parameter initial exciton number n_0 is shown in this figure.

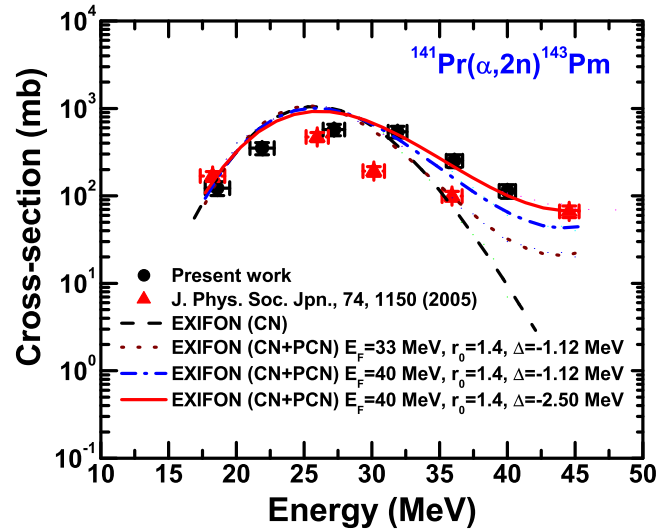

FIG. 13. The experimentally measured and theoretically calculated EFs for reaction ^{141}Pr$(\alpha, 2n)^{143}$Pm using code EXIFON. The effect of variation of parameter Δ on theoretical calculations is also shown in this figure.

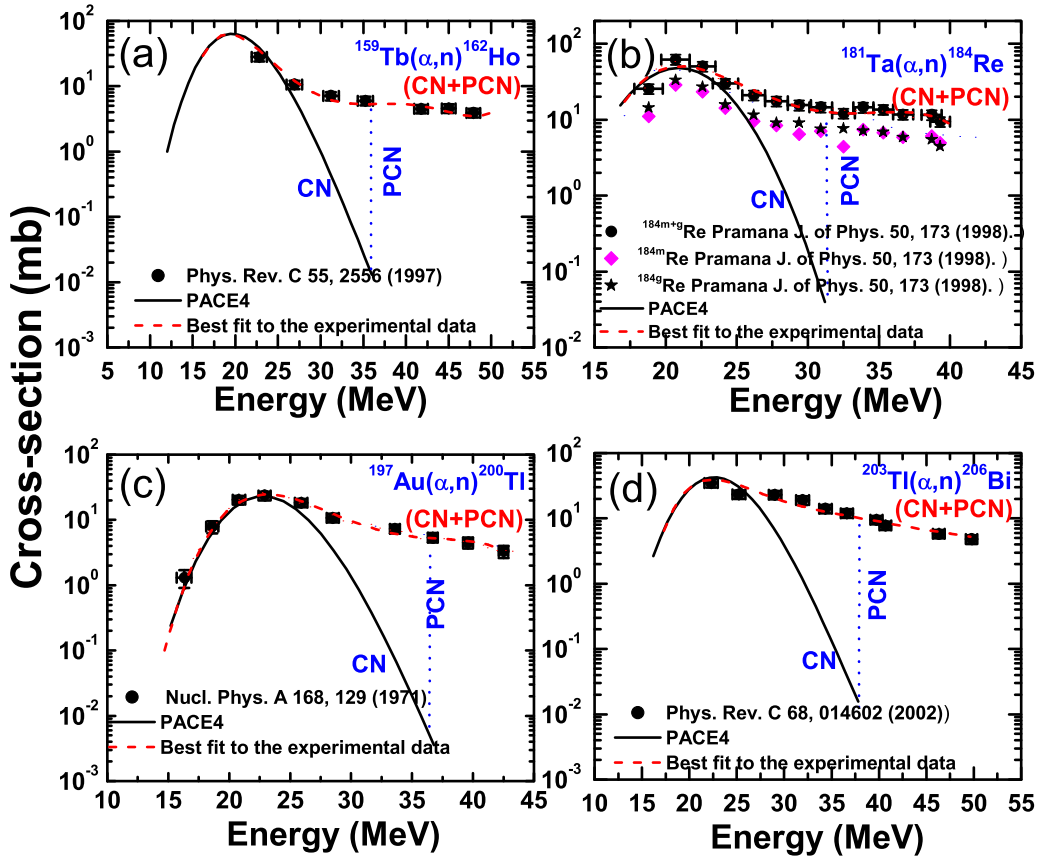

FIG. 14. The experimentally measured and theoretically calculated EFs for reactions ^{159}Tb$(\alpha, n)^{162}$Ho [74], ^{181}Ta$(\alpha, n)^{184}$Re [75,76], ^{197}Au$(\alpha, n)^{200}$Tl [77], and ^{203}Tl$(\alpha, n)^{206}$Bi [78], respectively, using code PACE4.

and ^{141}Pr$(\alpha, 2n)^{143}$Pm. From the above analysis it may be concluded that both the semiclassical as well as the QM codes, each with suitable choice of parameters, reproduce the experimental excitation functions satisfactorily. Further, PCN emission has been found to play an important role in α-induced reactions.

IV. SYSTEMATIC STUDY OF PRECOMPOUND EMISSION

Presently measured cross sections for the reactions ^{141}Pr$(\alpha, n)^{144}$Pm and ^{141}Pr$(\alpha, 2n)^{143}$Pm are in good agreement with theoretical calculations performed using different codes, viz., PACE, TALYS-1.9, ALICE91, ACT, and EXIFON, with a consistent set of parameters. It has been observed from the analysis of excitation functions for the $\alpha + ^{141}$Pr system that the precompound emission contribution competes with compound nucleus emission and its contribution increases with the projectile energy. In the literature, plenty of experimental data exist on α-particle-induced reactions with different target nuclei; however, there is hardly any systematic investigation of entrance channel effects in precompound emission. To develop a systematics on precompound emission in α-induced reactions, the experimental data of cross sections for one neutron reaction channel, ^{159}Tb$(\alpha, n)^{162}$Ho [74], ^{181}Ta$(\alpha, n)^{184}$Re [75,76], ^{197}Au$(\alpha, n)^{200}$Tl [77], and ^{203}Tl$(\alpha, n)^{206}$Bi [78], have been taken from the EXFOR data library [79]. These targets used in these reactions have odd Z and odd A similar to those used in the present work (^{141}Pr) so that the ambiguity, if any, arising due to odd-even effects of the target nuclei may be washed out. The theoretical calculations of EFs for the reactions ^{159}Tb$(\alpha, n)^{162}$Ho [74], ^{181}Ta$(\alpha, n)^{184}$Re [75,76], ^{197}Au$(\alpha, n)^{200}$Tl [77], and ^{203}Tl$(\alpha, n)^{206}$Bi [78] have been performed within the framework of the CN formalism by using the code PACE4 and are shown in Figs. 14(a) to Fig. 14(d). It can be seen from these figures that the predictions of the code PACE4 reproduce the experimental EFs for all these reactions up to their peak regions; however, beyond the peak region, i.e., in the tail portion of EFs, the observed difference between the measured data and theoretical calculations may be attributed to the contribution from precompound emission process. This is expected as the code PACE4 calculates the cross sections for compound nucleus emission and does not take the contribution of precompound emission into account. Thus, the precompound contribution for each of the above-mentioned reactions is deduced and discussed in the following subsection.

Precompound fraction f_{pe}

In order to perform a systematic study on precompound emission, the contribution of PCN in each reaction has been deduced in the form of precompound fraction f_{pe} which reflects the relative importance of such emission over compound nucleus emission. In the present work, the f_{pe} is

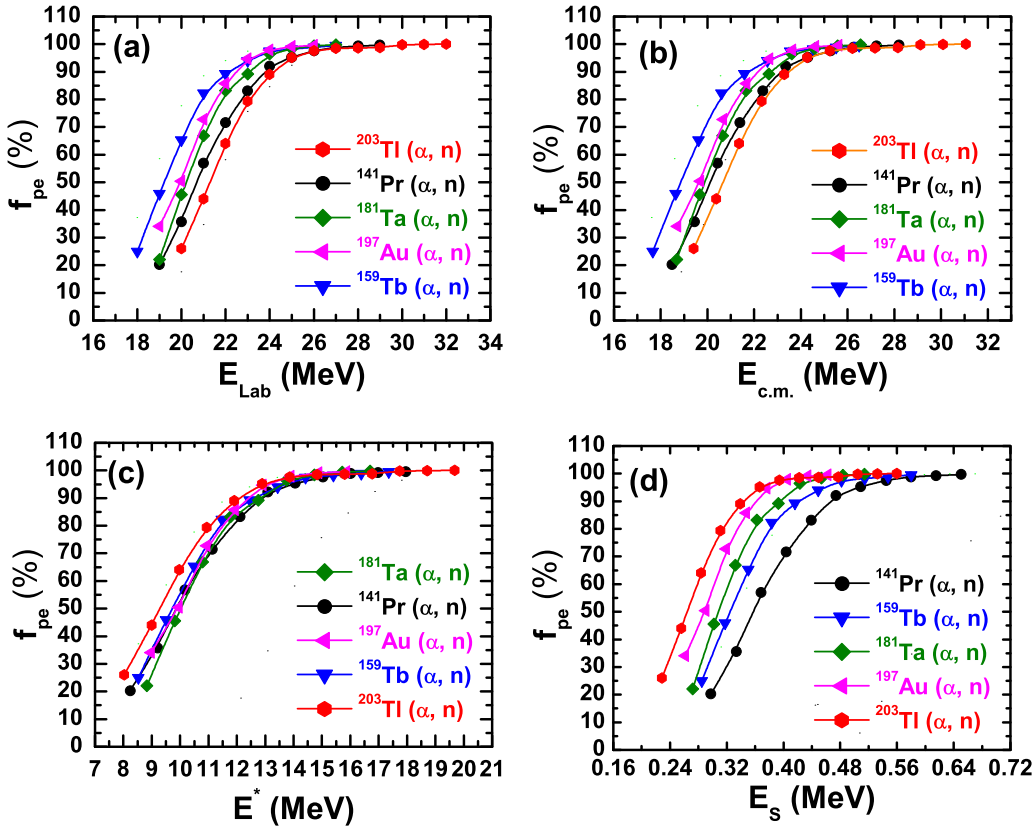

FIG. 15. The deduced f_{pe} as a function of laboratory energy (E_{lab}), center-of-mass energy ($E_{c.m.}$), excitation energy E^*, and excitation energy per surface nucleons E_S for the reactions ^{141}Pr$(\alpha, n)^{144}$Pm, ^{159}Tb$(\alpha, n)^{162}$Ho, ^{181}Ta$(\alpha, n)^{184}$Re, ^{197}Au$(\alpha, n)^{200}$Tl, and ^{203}Tl$(\alpha, n)^{206}$Bi, respectively.

deduced as the ratio of the deduced precompound contribution to the total CN+PCN contributions. The deduced f_{pe} values are plotted as a function of laboratory energy (E_{lab}), center-of-mass energy ($E_{c.m.}$), excitation energy (E^*), and excitation energy per surface nucleons of the composite nucleus E_S [$=(E^*/A^{2/3})$] for the reactions ^{141}Pr$(\alpha, n)^{144}$Pm, ^{159}Tb$(\alpha, n)^{162}$Ho, ^{181}Ta$(\alpha, n)^{184}$Re, ^{197}Au$(\alpha, n)^{200}$Tl, and ^{203}Tl$(\alpha, n)^{206}$Bi and are shown in Figs. 15(a) to 15(d). It can be seen from these figures that the deduced f_{pe} for these reactions increases rapidly with energy in each case. It has also been observed that a small variation in energy produces a large change in f_{pe} for the above reactions. This indicates that in case of precompound emission, the energy is a sensitive parameter as pointed out by Blann [56] in his pioneering study on precompound emission. From Figs. 15(a) and 15(b), it has observed that the f_{pe} attains maximum at different values of (E_{lab}) and ($E_{c.m.}$) for different target nuclei but no evidence of any systematic trend of f_{pe} with target mass has been observed.

Further, the values of deduced f_{pe} are plotted as a function of excitation energy E^* for the reactions ^{141}Pr$(\alpha, n)^{144}$Pm, ^{159}Tb$(\alpha, n)^{162}$Ho, ^{181}Ta$(\alpha, n)^{184}$Re, ^{197}Au$(\alpha, n)^{200}$Tl, and ^{203}Tl$(\alpha, n)^{206}$Bi and are shown in Fig. 15(c). The only observation which may be made in this case is that the value of the excitation energy at which f_{pe} begins is lower for the heavier target ^{203}Tl. However, there is no evidence of any systematic trend of PCN and target mass with respect to excitation energy.

As a matter of fact, in the precompound process, the emission of nucleons from the surface of the composite system is more feasible as compared to the nucleons well inside the nucleus. As such, the excitation energy per surface nucleon E_S of the composite system may be used as another parameter to characterize the PCN process. To get a systematic trend, the f_{pe} for the above systems are plotted as a function of E_S and are shown in Fig. 15(d). It can be seen from this figure that a systematic trend of the f_{pe} in terms of mass of the target nuclei and the excitation energy per surface nucleon of the composite system is observed. The contribution of precompound emission starts at a smaller value of E_S for the heaviest target ($A = ^{203}$Tl) and this trend follows systematically for lower-mass targets ($A = ^{141}$Pr) at relatively larger values of E_S. In other words, the value of E_S at which f_{pe} originates is higher for lower mass number of target and vice versa. This may indicate the key role of E_S in PCN process in such a way that all the nucleons of the composite system are not involved in such reaction mechanism. As such, the PCN emission may have a significant effect from the surface interactions. In other words, this may indicate that particles interacting in the nuclear periphery may have a better chance to be emitted as PCN particles, where an average lower density is present, as compared to the particles passing through the entire diameter

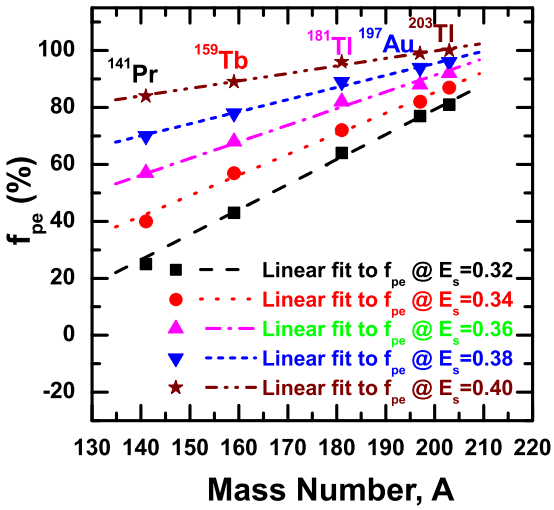

FIG. 16. Deduced precompound fraction f_{pe} of mass of the target nuclei as a function E_S.

of the target and therefore underlying the effect of the nuclear matter density region.

The information extracted from the above systematics [as given in Fig. 15(d)] may provide an insight for the PCN process for α-induced reactions and is depicted in Fig. 16. This figure shows variation of precompound fraction f_{pe} with mass number of target nuclei (A) at five different values of the E_S [=0.32 (shown by black square with dash line), 0.34 (red circle with line), 0.36 (magenta up-triangle with dash-dotted line), 0.38 (blue down-triangle with short-dashed line), and 0.40 (wine star with dash-dot-dotted line) MeV]. It can be seen from this figure that f_{pe} increases linearly with mass number at each value of E_S presently studied.

It may also be observed in Fig. 1 that fitted lines for different values of E_S which guide the deduced f_{pe} are not exactly parallel to each other but have different slopes. The slope of lines decreases with increase in the value of E_S. This means that the probability of PCN increases as mass of target nuclei increases at a given value of E_S. At higher values of the E_S, these lines start converging which indicates that the contribution of the PCN process saturates and becomes maximum for each target. As such, the systematics obtained in the present work throws additional insight on our existing understanding to the precompound emission process.

V. CONCLUSIONS

The excitation functions for reactions ^{141}Pr$(\alpha, n)^{144}$Pm and ^{141}Pr$(\alpha, 2n)^{143}$Pm have been measured in the energy range from threshold to ≈40 MeV. The measured excitation functions have been analyzed with a consistent set of parameters employing both the semiclassical codes (PACE4, TALYS-1.9, ACT, and ALICE91) and the quantum mechanical code EXIFON. It has been observed that experimentally measured excitation functions could be reproduced only when the precompound emission, simulated theoretically, is taken into account. The systematics obtained for precompound emission indicates that its strength deduced in terms of the precompound fraction f_{pe} sensitively depends on the excitation energy per surface nucleon (E_S) of the composite systems and mass number of the target nuclei. Further, as the value of E_S increases, the precompound contribution also increases in a systematic way, indicating that particles interacting in the nuclear periphery may have a better chance to be emitted as PCN particles, where an average lower density is present, as compared to the particles passing through the entire diameter of the target and therefore underlying the effect of the nuclear density matter region.

ACKNOWLEDGMENTS

The authors are thankful to the Director, VECC, Kolkata, India, for extending all the facilities for carrying out the experiments. One of the authors, M.K.S., thanks the Council of Scientific and Industrial Research (CSIR), New Delhi, Project No. 03(361)16/EMR-11, for financial support.

[1] B. P. Singh, H. D. Bhardwaj, and R. Prasad, Can. J. Phys. **69**, 1376 (1991).
[2] M. Avrigeanu, V. Avrigeanu, P. Bém, U. Fischer, M. Honusek, K. Katovsky, C. Mănăilescu, J. Mrázek, E. Simečková, and L. Zavorka, Phys. Rev. C **89**, 044613 (2014).
[3] K. Kim, G. N. Kim, H. Naik, M. Zaman, S.-C. Yang, T.-Y. Song, R. Guin, and S. K. Das, Nucl. Phy. A **935**, 65 (2015).
[4] M. K. Sharma, H. D. Bhardwaj, Unnati, P. P. Singh, B. P. Singh, and R. Prasad, Eur. Phys. J. A **31**, 43 (2007).
[5] B. P. Singh, Manoj K. Sharma, M. M. Muthafa, H. D. Bhardwaj, and R. Prasad, Nucl. Instrum. Methods Phys. Res., Sect. A **562**, 717 (2006).
[6] J. Pal, S. Saha, C. C. Dey, P. Banerjee, S. Bose, B. K. Sinha, M. B. Chatterjee, and S. K. Basu, Phys. Rev. C **71**, 034605 (2005).
[7] S. Mukherjee, N. L. Singh, G. K. Kumar, and L. Chaturvedi, Phys. Rev. C **72**, 014609 (2005).
[8] J. R. Wu, C. C. Chang, and H. D. Holmgren, Phys. Rev. C **19**, 659 (1979).
[9] T. C. Awes, G. Poggi, C. K. Gelbke, B. B. Back, B. G. Glagola, H. Breuer, and V. E. Viola, Jr., Phys. Rev. C **24**, 89 (1981).
[10] J. Luo, L. Jiang, and S. Li, Phys. Rev. C **96**, 044617 (2017).
[11] M. K. Sharma, P. P. Singh, D. P. Singh, A. Yadav, V. R. Sharma, I. Bala, R. Kumar, Unnati, B. P. Singh, and R. Prasad, Phys. Rev. C **91**, 014603 (2015).
[12] E. Gadioli, E. Gadioli-Erba, J. J. Hogan, and B. V. Jacak, Phys. Rev. C **29**, 76 (1984).
[13] J. Ernst, W. Friedland, and H. Stockhorst, Z. Phys. A: At. Nucl. **328**, 333 (1987).
[14] J. Ernst, W. Friedland, and H. Stockhorst, Z. Phys. A: At. Nucl. **308**, 301 (1982).
[15] S. Sudar and S. M. Qaim, Phys. Rev. C **73**, 034613 (2006).
[16] B. P. Singh, M. G. V. Sankaracharyulu, M. A. Ansari, H. D. Bhardwaj, and R. Prasad, Phys. Rev. C **47**, 2055 (1993).

[17] C. Rubbia, J. A. Rubbio, S. Buono *et al.*, Conceptual Design of a Fast Neutron Operated High Power Energy Amplifier, Report CERN/AT/95-94 (ET), 1995.
[18] A. Gavron, Phys. Rev. C **21**, 230 (1980).
[19] PACE4 code, http://lise.nscl.msu.edu/pace4.
[20] A. J. Koning, S. Hilaire, and S. Goriely, TALYS User Manual, A Nuclear Reaction Program, NRG-1755 ZG Petten, The Netherlands, 2015.
[21] H. D. Bhardwaj, Ph.D. thesis, A. M. U. Aligarh, India, 1985.
[22] M. Uhl and B. Strohmair, Report IRK 76/01, NEA Data Bank, France, 1981.
[23] M. Blann, Report PSR-146, NEA Data Bank, Gif-sur-Yvette, France, 1991.
[24] H. Kalka, ExIFQN, A Statistical Multistep Reaction Code, NEA Data Bank, Saclay, France, 1991.
[25] O. Lebeda, V. Lozza, J. Petzoldt, J. Stursa, V. Zdychova, and K. Zuber, Nucl. Phys. A **929**, 129 (2014).
[26] F. Tarkanyi, S. Takacs, F. Ditroi, A. Hermanne, H. Yamazaki, M. Baba, A. Mohammadi, and A. V. Ignatyuk, Nucl. Instrum. Methods Phys. Res., Sect. B **325**, 15 (2014).
[27] A. Sauerwein, H. W. Becker, H. Dombrowski, M. Elvers, J. Endres, U. Giesen, J. Hasper, A. Hennig, L. Netterdon, T. Rauscher, D. Rogalla, K. O. Zell, and A. Zilges, Phys. Rev. C **84**, 045808 (2011).
[28] M. Afzal Ansari, N. P. M. Sathik, D. Singh, and M. H. Rasid, J. Phys. Soc. Jpn. **74**, 1150 (2005).
[29] See http://www.srim.org.
[30] E. Browne and R. B. Firestone, *Table of Radioactive Isotopes* (Wiley, New York, 1986).
[31] H. Feshbach, A. Kerman, and R. Lemmer, Ann. Phys. **41**, 280 (1967).
[32] K. Debertin and R. G. Helmer, *Gamma- and X-Ray Spectroscopy with Semiconductor Detectors* (North-Holand, Netherlans, 1988).
[33] T. Udagawa, K. S. Low, and T. Tamura, Phys. Rev. C **28**, 1033 (1983).
[34] D. Agassi, H. A. Weidenmuller, and G. Mantzouranis, Phys. Rep. **22**, 145 (1975).
[35] R. Bass, Nucl. Phys. A **231**, 45 (1974).
[36] B. Lawriniang, R. Ghosh, S. Badwar, V. Vansola, Y. Santhi Sheela, S. V. Suryanarayana, H. Naik, Y. P. Naik, and B. Jyrwa, Nucl. Phys. A **973**, 79 (2018).
[37] S. Parashari, S. Mukherjee, B. K. Nayak, R. Makwana, S. V. Suryanarayana, H. Naik, and S. C. Sharma, Nucl. Phys A **978**, 160 (2018).
[38] S. Parashari, S. Mukherjee, R. Makwana, B. K. Nayak, A. Shanbhag, and H. Naik, Nucl. Phys A **979**, 102 (2018).
[39] R. Capote *et al.*, Nucl. Data Sheets **110**, 3107 (2009).
[40] A. J. Koning and J. P. Declaroche, Nucl. Phys. A **713**, 231 (2003).
[41] W. Hauser and H. Feshbach, Phys. Rev. **87**, 366 (1952).
[42] C. Kalbach, Phys. Rev. C **33**, 818 (1986).
[43] A. Gilbert and A. G. W. Cameron, Can. J. Phys. **43**, 1446 (1965).
[44] W. Dilg, W. Schantl, H. Vonach, and M. Uhl, Nucl. Phys. A **217**, 269 (1973).
[45] A. V. Ignatyuk, K. K. Istekov, and G. N. Smirenkin, Sov. J. Nucl. Phys. **29**, 450 (1979).
[46] A. V. Ignatyuk, J. L. Weil, S. Raman, and S. Kahane, Phys. Rev. C **47**, 1504 (1993).
[47] S. Goriely, S. Hilaire, and A. J. Koning, Phys. Rev. C **78**, 064307 (2008).
[48] S. Hilaire, M. Girod, S. Goriely, and A. J. Koning, Phys. Rev. C **86**, 064317 (2012).
[49] D. W. Lang, Nucl. Phys. **77**, 545 (1966).
[50] M. Blann and H. K. Vonach, Phys. Rev. C **28**, 1475 (1983).
[51] A. H. Wapstra and K. Bos, At. Data Nucl. Data Tables **19**, 215 (1977).
[52] F. C. Williams, Jr., Phys. Lett. B **31**, 353 (1970).
[53] C. K. Cline, Nucl. Phys. A **186**, 273 (1972).
[54] H. Jahn, Nuclear Theory for Applications, IAER-SMR-93, 39, 1982.
[55] C. Kalbach-Cline, Nucl. Phys. A **210**, 590 (1973).
[56] M. Blann, Phys. Rev. Lett. **27**, 337 (1971).
[57] V. F. Weisskopf and D. H. Ewing, Phys. Rev. **57**, 472 (1940).
[58] W. D. Myers and W. J. Swiatecki, Ark. Fys. **36**, 343 (1967).
[59] M. Blann, Phys. Rev. C **21**, 1770 (1980).
[60] F. D. Becchetti and G. W. Greenlees, Phys. Rev. **182**, 1190 (1969).
[61] K. Kikuchi and M. Kawai, *Nuclear Matter and Nuclear Reactions* (North-Holland Publishing Co., Amsterdam, 1968).
[62] M. Blann, Nucl. Phys. A **213**, 570 (1973).
[63] J. R. Huizenga and L. G. Moretto, Annu. Rev. Nucl. Sci. **22**, 427 (1972).
[64] H. Feshbach, A. K. Kerman, and S. Koonin, Ann. Phys. (N.Y.) **125**, 429 (1980).
[65] C. Kalbach-Cline, J. R. Huizenga, and H. K. Vonach, Nucl. Phys. A **222**, 405 (1974).
[66] C. D. Coryell, Annu. Rev. Nucl. Sci. **2**, 331 (1953).
[67] C. K. Cline and M. Blann, Nucl. Phys. A **172**, 255 (1971).
[68] C. Kalbach, Z. Phys. A **283**, 401 (1977).
[69] C. Kalbach, Z. Phys. A **287**, 319 (1978).
[70] C. Kalbach, Z. Phys. A **332**, 397 (1989).
[71] P. Oblozinsky, Phys. Rev. C **40**, 1591 (1989).
[72] M. Avrigeanu and V. Avrigeanu, J. Phys. G **20**, 613 (1994).
[73] M. Avrigeanu, M. Ivascu, and V. Avrigeanu, Z. Phys.- Atomic Nuclei A **335**, 299 (1990).
[74] S. Mukherjee, B. Bindu Kumar, M. H. Rashid, and S. N. Chintalapudi, Phys. Rev. C **55**, 2556 (1997).
[75] M Ismail, Pramana **50**, 173 (1998).
[76] N. E. Scott, J. W. Cobble, and P. J. Daly, Nucl. Phys. A **119**, 131 (1968).
[77] H. E. Kurz, E. W. Jasper, K. Fisscher, and F. Hermes, Nucl. Phys. A **168**, 129 (1971).
[78] N. P. M. Sathik, M. Afzal Ansari, B. P. Singh, M. Ismail, and M. H. Rashid, Phys. Rev. C **66**, 014602 (2002).
[79] EXFOR: Experimental Nuclear Reactions, http://www-nds.iaea.org/exfor/.